PARTICLE PRODUCTION AS A FUNCTION OF UNDERLYING-EVENT ACTIVITY AND SEARCH FOR JET-LIKE MODIFICATIONS IN pp, p–Pb, AND Pb–Pb COLLISIONS AT $\sqrt{s_{NN}} = 5.02$ TeV WITH ALICE*

Antonio Ortiz

for the ALICE Collaboration

CERN, 1211 Geneva 23, Switzerland
and
UNAM, Apartado Postal 70-543, Ciudad de México 04510, México

Received 21 July 2022, accepted 22 September 2022, published online 14 December 2022

The charged-particle multiplicity in the transverse region, $N_{\mathrm{ch}}^{\mathrm{T}}$, which is sensitive to the underlying event, is studied. Measurements of charged-particle production as a function of $N_{\mathrm{ch}}^{\mathrm{T}}$ in pp, p–Pb, and Pb–Pb collisions at $\sqrt{s_{NN}} = 5.02$ TeV in the toward, away, and transverse regions are discussed. These regions are defined relative to the track with the largest transverse momentum in the event ($p_{\mathrm{T}}^{\mathrm{trig}}$). The activity in the transverse region is subtracted from the activity in the toward and away regions to search for jet-like modifications in small collision systems. The jet-like signals are studied both as a function of $N_{\mathrm{ch}}^{\mathrm{T}}$ and $p_{\mathrm{T}}^{\mathrm{trig}}$. Results are compared with two general-purpose Monte Carlo event generators: PYTHIA 8 and EPOS LHC.

DOI:10.5506/APhysPolBSupp.16.1-A61

1. Introduction

In models incorporating multi-parton interactions (MPI), particles produced in the hard scattering (jet) are accompanied by particles from additional parton–parton interactions, as well as from the proton break-up [1]. This component of the collision makes up the underlying event (UE). The traditional UE analysis focuses on the study of particles in three topological regions depending on their azimuthal angle relative to the leading particle ($|\Delta\varphi| = |\varphi - \varphi^{\mathrm{trig}}|$), which is the one with the highest transverse momentum in the event ($p_{\mathrm{T}}^{\mathrm{trig}}$). The toward region ($|\Delta\varphi| < \pi/3\,\mathrm{rad}$) contains the

* Presented at the 29$^{\mathrm{th}}$ International Conference on Ultrarelativistic Nucleus–Nucleus Collisions: Quark Matter 2022, Kraków, Poland, 4–10 April, 2022.

primary jet and UE, while the away region ($\pi/3\,\mathrm{rad} < |\Delta\varphi| < 2\pi/3\,\mathrm{rad}$) contains the fragments of the recoil jet and UE. In contrast, the transverse region ($|\Delta\varphi| > 2\pi/3\,\mathrm{rad}$) is dominated by the UE dynamics, but it also includes contributions from initial- and final-state radiation [2]. High-energy *pp* and *p*–Pb collisions (small collision systems) unveiled remarkable similarities with heavy-ion collisions like collectivity, and strangeness enhancement. In heavy-ion collisions, such effects are attributed to the formation of the strongly interacting quark–gluon plasma (sQGP) [3]. This work discusses new results aiming at understanding small collision systems using UE-inspired techniques [4–7], with special emphasis on quantities which by construction are expected to be sensitive to jet quenching.

2. Experimental setup and data analysis

The V0 detector is used for triggering and background rejection, it consists of two arrays of scintillating tiles covering the pseudorapidity intervals of $2.8 < \eta < 5.1$ (V0A) and $-3.7 < \eta < -1.7$ (V0C). For *pp* and Pb–Pb collisions, the sample is subdivided into different multiplicity classes based on the total charge deposited in both V0 sub-detectors (V0M amplitude). For *p*–Pb collisions, the sample is subdivided based on the total charge deposited in the V0A sub-detector (V0A amplitude).

The p_{T} spectra are measured in the central barrel with the Inner Tracking System and the Time Projection Chamber following the standard procedure of the ALICE Collaboration [8]. Tracks are selected in the kinematic ranges $p_{\mathrm{T}} > 0.5\,\mathrm{GeV}/c$ and $|\eta| < 0.8$. The raw yields as a function of $p_{\mathrm{T}}^{\mathrm{trig}}$ or the activity in the V0 detector are corrected for efficiency and contamination from secondary particles. Another correction which is relevant for $p_{\mathrm{T}}^{\mathrm{trig}} < 5\,\mathrm{GeV}/c$ is the leading track misidentification correction which is described in Ref. [4]. The main sources of systematic uncertainties include: (1) track selection criteria, (2) imperfect simulation of the detector response, (3) secondary particle contamination, (4) leading track misidentification, and (5) a correction method.

3. Results and discussion

Figure 1 shows the number density as a function of $p_{\mathrm{T}}^{\mathrm{trig}}$ measured in *pp* and *p*–Pb collisions. Results are presented for the toward, transverse, and away regions. The $p_{\mathrm{T}}^{\mathrm{trig}}$ dependence in all regions is similar for both collision systems. For $p_{\mathrm{T}}^{\mathrm{trig}} < 5\,\mathrm{GeV}/c$, the number densities exhibit a steep rise with increasing $p_{\mathrm{T}}^{\mathrm{trig}}$. For higher $p_{\mathrm{T}}^{\mathrm{trig}}$ the increases are less steep. The effect is more pronounced for the transverse region, where the number density is almost independent of $p_{\mathrm{T}}^{\mathrm{trig}}$. The remarkable similarity between *pp* and *p*–Pb

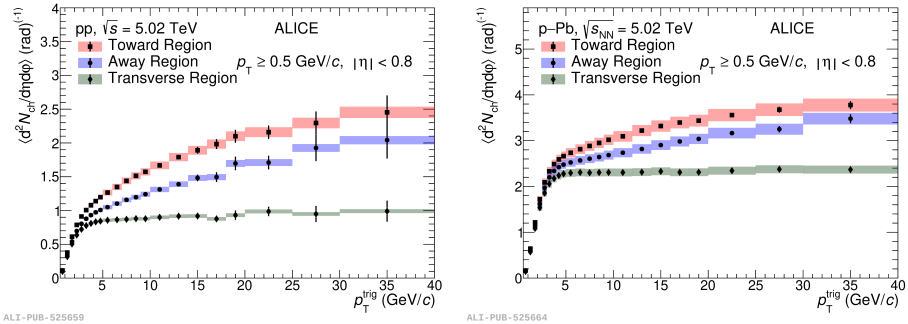

Fig. 1. Number density as a function of $p_{\mathrm{T}}^{\mathrm{trig}}$ measured in *pp* (left) and *p*–Pb collisions (right) at $\sqrt{s_{NN}} = 5.02\,\mathrm{TeV}$. Results for the toward, transverse, and away regions are displayed.

collisions indicates a similar bias in the *pp* and *p*–Pb impact parameter, and to some extent, in the nucleon–nucleon impact parameter [9]. On the other hand, the rise of the number density observed for the toward and away regions is due to the contribution from the jet fragments.

In order to increase the sensitivity to the particles produced in the hard scattering, jet-like signals are obtained from the number density in the toward and away regions after subtracting the number density in the transverse region. Figure 2 shows the jet-like contribution to the number density in the toward and away regions as a function of $p_{\mathrm{T}}^{\mathrm{trig}}$ for *pp* and *p*–Pb collisions at $\sqrt{s_{NN}} = 5.02\,\mathrm{TeV}$. The number densities in the jet-like signals rise with increasing $p_{\mathrm{T}}^{\mathrm{trig}}$ in the entire range of the measurement. At high $p_{\mathrm{T}}^{\mathrm{trig}}$ ($> 10\,\mathrm{GeV}/c$), the number density exhibits a remarkable similarity between *pp* and *p*–Pb collisions. Within 10%, both PYTHIA 8 Angantyr [10] and EPOS LHC reproduce this feature. This is consistent with the absence of medium effects in minimum-bias *p*–Pb collisions at high $p_{\mathrm{T}}^{\mathrm{trig}}$. At lower $p_{\mathrm{T}}^{\mathrm{trig}}$, the models overestimate the number density in *p*–Pb collisions. The disagreement is more remarkable for EPOS LHC than for PYTHIA 8 Angantyr. The number density in *pp* collisions scaled to that in *p*–Pb collisions is smaller than unity, reaching a minimum of ≈ 0.8 at $p_{\mathrm{T}}^{\mathrm{trig}} \approx 3\,\mathrm{GeV}/c$. This behaviour is not reproduced by PYTHIA 8 Angantyr. In contrast, EPOS LHC exhibits a similar pattern, but the size of the effect is much larger than in the data. The main difference between PYTHIA 8 Angantyr and EPOS LHC is that EPOS LHC incorporates collective flow.

To further investigate the possible modification of the particles produced in the hard scattering using *pp* and *p*–Pb data, only collisions containing a leading track transverse momentum within $8 < p_{\mathrm{T}}^{\mathrm{trig}} < 15\,\mathrm{GeV}/c$ are considered. Moreover, small collision systems are compared with Pb–Pb collisions

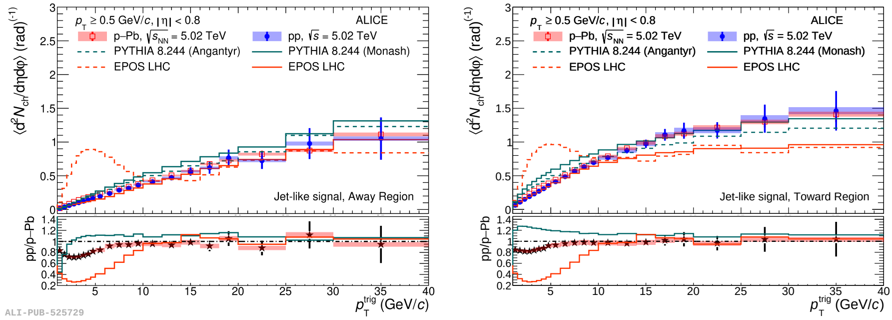

Fig. 2. Number density as a function of $p_{\mathrm{T}}^{\mathrm{trig}}$ in *pp* and *p*–Pb collisions. Results for the away (left) and toward (right) regions are shown. The *pp* results scaled to the *p*–Pb ones are shown in the bottom panel.

at the same centre-of-mass energy per nucleon pair, where there is enough evidence of medium-jet modifications due to the presence of sQGP. The high-p_{T} yields ($4 < p_{\mathrm{T}} < 6\,\mathrm{GeV}/c$) in the toward ($Y^{\mathrm{t}}$) and away ($Y^{\mathrm{a}}$) regions obtained after the subtraction of the high-p_{T} yield in the transverse region (Y^{T}) are measured. The subtracted yields ($Y^{\mathrm{st,sa}}$) are further normalised to those measured in minimum-bias (MB) *pp* collisions. With these quantities, the $I_X^{\mathrm{t,a}}$ factors are defined as $I_X^{\mathrm{t,a}} \equiv (Y_X^{\mathrm{t,a}} - Y_X^{\mathrm{T}})/(Y_{pp,\mathrm{MB}}^{\mathrm{t,a}} - Y_{pp,\mathrm{MB}}^{\mathrm{T}}) = Y_X^{\mathrm{st,sa}}/Y_{pp,\mathrm{MB}}^{\mathrm{st,sa}}$, where X indicates the collision system and the event multiplicity class. In the absence of medium effects or selection biases, this quantity is expected to be consistent with unity.

Figure 3 shows $I_X^{\mathrm{t,a}}$ as a function of $\langle N_{\mathrm{ch}}^{\mathrm{T}} \rangle$ for *pp*, *p*–Pb, and Pb–Pb collisions. Data are compared with PYTHIA 8 and EPOS LHC. As discussed earlier, the events were classified in terms of the activity in the V0 detector. This reduces the presence of particles from hard Bremsstrahlung gluons that can contribute to the transverse region [11]. Within uncertainties, the $I_X^{\mathrm{t,a}}$ values are close to unity for all the multiplicity classes measured in *pp* collisions. The small multiplicity dependence observed in *pp* collisions is due to selection biases, the effect is reproduced by PYTHIA 8 that does not incorporate any jet quenching mechanism. The results indicate that effects induced by possible energy loss in *pp* collisions are not observed.

For *p*–Pb collisions, within uncertainties, the $I_X^{\mathrm{t,a}}$ values are close to unity for all the multiplicity classes suggesting the absence of medium effects. The data are compared to PYTHIA 8 Angantyr [10] and EPOS LHC predictions [12]. The Angantyr model predicts the I_X^{a} factor to be consistent with unity, and I_X^{t} slightly below unity. On the other hand, EPOS-LHC describes neither the magnitude nor the trend of the multiplicity dependence of the measured ratio in the toward region, I_X^{t}. However, the model is in reasonable agreement with data in the away region.

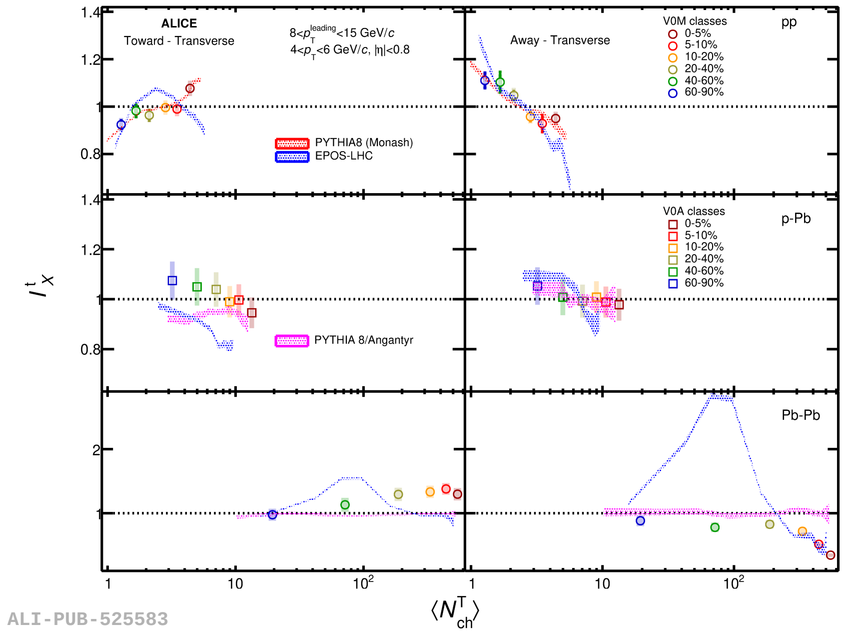

Fig. 3. Comparison of $I_X^{\rm t}$ (left) and $I_X^{\rm a}$ (right) with model predictions. The results are shown as a function of $\langle N_{\rm ch}^{\rm T}\rangle$ for different multiplicity classes in *pp* (top panel), *p*–Pb (middle panel), and Pb–Pb (bottom panel) collisions.

By contrast, for Pb–Pb collisions the $I_X^{\rm t,a}$ values are compatible with unity for peripheral collisions, and show a gradual increase (reduction) with the increase in multiplicity for the toward (away) region. The behaviour is the same even considering the modulation of the underlying event by elliptic flow (v_2). On the one hand, the suppression in the away region is expected from the strong in-medium energy loss; on the other hand, the enhancement observed in the toward region is also subject to medium effects [13]. Regarding the model comparisons, PYTHIA 8 Angantyr predicts $I_X^{\rm t,a}$ values consistent with unity for all the multiplicity classes and EPOS LHC predicts a significant enhancement of $I_X^{\rm t,a}$ for low $\langle N_{\rm ch}^{\rm T}\rangle$ ranges and deviates significantly from the experimental results.

4. Conclusions

For the first time, the properties of the underlying event are measured in collisions involving heavy ions. The charged-particle densities as a function of $p_{\rm T}^{\rm trig}$ exhibit a saturation at $p_{\rm T}^{\rm trig} \approx 5\,{\rm GeV}/c$ in the transverse region for both *pp* and *p*–Pb collisions at $\sqrt{s_{NN}} = 5.02\,{\rm TeV}$. The charged-particle density in the toward and away regions are studied after subtracting the number density in the transverse region. While the data from Pb–Pb collisions are in agreement with expectations from parton energy loss due to the presence of a hot and dense medium, *pp* and *p*–Pb data do not show any hint of medium effects in the multiplicity and p_{T} ranges which are reported.

This work has been supported by CONACyT under the grants CB No. A1-S-22917 and CF No. 2042, as well as by PASPA-DGAPA UNAM.